Optimal Co-planning of ESSs and Line Reinforcement considering the Dispatchability of Active Distribution Networks

Ji Hyun Yi, Rachid Cherkaoui, *Senior Member, IEEE,* Mario Paolone, *Fellow, IEEE,*
Dmitry Shchetinin, *Member, IEEE,* Katarina Knezovic, *Member, IEEE,*

***Abstract*—The paper presents a method for the co-optimization of energy storage systems allocation and line reinforcement in active distribution networks. The objective is to guarantee the capability of an active distribution network to follow a dispatch plan by appropriately coping with the high uncertainties of loads and stochastic renewable generation while ensuring the secure operation of the grid and minimizing the power grid losses. The proposed formulation relies on a modified formulation of the so-called Augmented Relaxed Optimal Power Flow (AR-OPF) method, which considers the exact (*i.e.*, non-approximated) AC-OPF in a convexified way (the AR-OPF is proven to provide the global optimal and exact solution of the OPF problem for radial power grids). To tackle the complexity and computational burden of the proposed planning problem, the Benders decomposition algorithm is used and, in order to enhance the convergence speed of the numerical solution of the proposed problem, the Benders decomposition has been suitably modified to determine the energy storage systems site and size sequentially. To assess the performance of the proposed method, simulations are conducted on a real Swiss distribution network composed of 55 nodes and hosting a large amount of stochastic photovoltaic generation. The sensitivity analysis with respect to the photovoltaic capacity is also carried out to assess the effectiveness of the proposed method.**

***Index Terms*—Active distribution networks, dispatchability, energy storage systems, line reinforcement, optimal power flow, Benders decomposition.**

NOMENCLATURE

Sets and Indices

$l \in \mathcal{L}$	Indices of buses or indices of lines connected upstream
$y \in \mathcal{Y}$	Indices and set of years
$d \in \mathcal{D}$	Indices and set of days
$t \in \mathcal{T}$	Indices and set of time intervals
$\phi \in \Phi_{dy}$	Indices and set of scenarios for day d and year y
$n \in \mathcal{N}_1 \backslash \mathcal{N}_2$	Indices and set of Benders iterations for 1st\2nd stage problem of 2nd block problem
$m \in \mathcal{M}_1 \backslash \mathcal{M}_2$	Indices and set of iteration number of the 1st\2nd stage subproblem of 2nd block problem

Variables

$U_l \in \{0,1\}$	Installation status of the ESS at bus l
C_l	Energy reservoir of the ESS at bus l
R_l	Power rating of the ESS at bus l
$X_l \in \{0,1\}$	Reinforcement status of line l
A_l	Updated ampacity of line l
ΔA_l	Change in ampacity of line l
IC	Total investment cost
IC_E	Investment cost of energy storage system assets
IC_L	Investment cost of line reinforcement
$MC^1 \backslash MC^2$	Master problem cost of 1st and 2nd stage of 2nd block problem
$SC^1_{dy} \backslash SC^2_{dy}$	Subproblem cost of day d and year y of 1st and 2nd stage of 2nd block problem
$\tilde{p}_{ltdy}$	Average of the active load over all scenarios at: bus l, time t, day d, and year y
$\Delta p_{l\phi t}$	Deviation of prosumption from $\tilde{p}_{ltdy}$ at: bus l, scenario ϕ, and time t
$\tilde{f}_{ltdy}$	Average of squared longitudinal current causing losses over all scenarios at: line l, time t, day d, and year y
$\Delta f_{l\phi t}$	Deviation of squared longitudinal current causing losses from $\tilde{f}_{ltdy}$ at: bus l, scenario ϕ, and time t
DP_{tdy}	Dispatch plan associated with time t, day d, and year y at the grid connecting point (GCP)
$\epsilon_{l\phi t}$	Uncovered dispatch error at: bus l, scenario ϕ, and time t
$\theta_{\phi t}$	Leftover dispatch error rate for scenario ϕ, time t
$f_l \backslash \bar{f}_l$	Square of longitudinal current magnitude causing losses in line l\Auxiliary upper bound variable
$v_l \backslash \bar{v}_l$	Square of voltage magnitude at bus l\Auxiliary upper bound variable
$s_l = p_l + jq_l$	Aggregated prosumption at bus l
$S^t_l = P^t_l + jQ^t_l$	Upstream complex power flow to line l
$\bar{S}^t_l = \bar{P}^t_l + j\bar{Q}^t_l$	Auxiliary variable of upstream complex power flow to line l (upper bound of S^t_l)
$\hat{S}^t_l = \hat{P}^t_l + j\hat{Q}^t_l$	Auxiliary variable of upstream complex power flow to line l (lower bound of S^t_l)
$S^b_l = P^b_l + jQ^b_l$	Downstream complex power flow to bus l from line l
$\bar{S}^b_l = \bar{P}^b_l + jQ^b_l$	Auxiliary variable of complex power flow to bus l from line l (upper bound of S^b_l)
$\hat{S}^b_l = \hat{P}^b_l + j\hat{Q}^b_l$	Auxiliary variable of complex power flow to bus l from line l (lower bound of S^b_l)
$s^E_l = p^E_l + jq^E_l$	Complex power flow of ESS at bus l
$E^E_{l\phi t}$	Energy stored in the ESS installed at bus l, scenario ϕ, and time t
$up^+_{l\phi t} \backslash up^-_{l\phi t}$	Positive\negative unserved active load at: bus l, scenario ϕ, and time t
$uq^+_{l\phi t} \backslash uq^-_{l\phi t}$	Positive\negative unserved reactive load at: bus l, scenario ϕ, and time t
$\gamma^m_{\phi t}, \zeta^m_{\phi t}$	Slack variables representing approximation of losses deviation value at m^{th} iteration of solving subproblem of 1st/2nd stage of 2nd block problem for scenario ϕ and time t

Parameters

λ_ϕ	Probability of scenario ϕ
T	Time horizon of the daily OPF problem

Ji Hyun Yi, Rachid Cherkaoui, Mario Paolone are with the Distributed Electrical Systems Laboratory, École Polytecnique Fédérale de Lausanne (EPFL), Lausanne, Switzerland (e-mail: ji.yi@epfl.ch; rachid.cherkaoui@epfl.ch; mario.paolone@epfl.ch).

Dmitry Shchetinin and Katarina Knezovic are with Hitachi Energy Research, Baden Dättwil, Switzerland (e-mail: dmitry.shchetinin@hitachienergy.com; katarina.knezovic@hitachienergy.com.)

Δt	Time duration of dispatch interval
Y	Planning horizon
N_{dy}	Number of days in day-type d in year y
G	Network adjacency matrix
b_l	Half of the total shunt susceptance of line l
z_l=r_l+jx_l	Total longitudinal impedance of line l
I_l^{max}	Upper limit on the current of line l
$P_l^{max}\backslash Q_l^{max}$	Upper limits of active\reactive power flows for line l, respectively
$v^{max}\backslash v^{min}$	Upper bounds\Lower bounds of the squared nodal voltage magnitude
ic_E^f, ic_E^e, ic_E^p	Investment cost parameter for ESS installation, energy reservoir, power rating
ic_l^r	Fixed cost parameter for line reinforcement of line l
$\delta_2, \delta_1, \delta_0$	Coefficient for quadratic, linear, constant term of line conductor cost function with respect to line ampacity, respectively
ρ_l	Line length of line l
$A^{max}\backslash A^{min}$	Maximum\minimum possible ampacity of line conductor
ΔA^{max}	Maximum possible change in ampacity of line conductor
$C_l^{max}\backslash C_l^{min}$	Maximum\minimum possible ESS energy reservoir capacity at bus l
$R_l^{max}\backslash R_l^{min}$	Maximum\minimum possible ESS power rating capacity at bus l
CR^{max}	Maximum power ramping rate of ESS
$E^{max}\backslash E^{min}$	Maximum\minimum allowed state-of-energy level
E_{ini}	Initial level of ESS state-of-energy level
Δ^f	Maximum difference between the final and initial state-of-energy level with respect to the ESS energy reservoir capacity
$\alpha_l, \beta_l, \kappa_l$	Vectors defining the slope and the intercepts, respectively, of the set of lines which approximate the power capability curve of ESS at bus l
N_c	Allowed number of cycles per day chosen as a function of the targeted ESS lifetime
w_d, w_l, w_u	Weight coefficient associated to the error between the dispatch plan and the active slack power in each scenario, grid losses, unserved load, respectively
r_i	Discount rate
Function	
$L(x)$	Piecewise linearization of x

I. Introduction

THE progressive connection of stochastic renewable generation into power distribution systems increases the uncertainty of the electricity production of the whole generation mix, posing a severe challenge regarding its reliable dispatch [1]. Indeed, the stochastic nature of the power generation connected to distribution systems is propagated into the upper-level grid, making the power balancing more challenging for transmission systems operators (TSOs). In this respect, distribution systems operators (DSOs) have been called for financial responsibility concerning power imbalances they may produce [2]–[4]. Accordingly, relevant regulatory changes into the power market have been proposed with incentive and penalty mechanisms for DSOs to promote the reliable balancing and dispatching of their networks [3] while supporting TSOs' balancing operation [4].

Several works in the recent literature have tried to address this problem. In [5], [6], it is proposed to make use of active controllable resources, such as energy storage systems (ESSs) connected to active distribution networks (ADNs) to limit DSOs' financial risks caused by power imbalances due to ADNs' unreliable dispatch. In particular, these works used ESSs to achieve the dispatchability of ADNs, which consist of tracking a day-ahead computed power profile at the grid connection point (GCP) with the upper-grid layer (usually represented by the ADN's connection to the sub-transmission grid). This specific setup has been named *dispatchability-by-design* in [7] and it is quantified how this setup may reduce the whole grid's reserve requirement [7], [8].

Although ADNs *dispatchability-by-design* is not yet employed in practice[1], the necessity of modifying regulatory frameworks has been pointed out in several studies [10]–[12]. In this context, reasonable assumptions can be applied to DSOs that operate ADNs: (i) the DSO is financially responsible for the energy imbalance caused by its electric power systems, (ii) ESSs can be owned and operated by the DSO to mitigate financial risks in the power market and not for power arbitrage. Under these assumptions, it is worthwhile for DSOs to consider the investment and deployment of the ESSs within their planning strategies.

In this regard, the authors of this work have proposed in [13] a planning methodology to optimally site and size ESSs in ADNs to achieve their dispatchability while accounting for the grid constraints and scenarios modeling the stochastic generation and loads over the planning horizon. In [13], it is shown how the allocation (determining sites and sizes) of ESSs may be largely influenced by binding grid constraints with a particular reference to line ampacity. In view of the above, the planning considering ESSs as the sole resource for DSOs may result in a sub-optimal solution. Instead, the ADNs asset investments may also take into account the line reinforcement. Conventionally, DSOs have tackled the operational issues associated with ADNs hosting capacity [2] by standard line reinforcement schemes as presented in [14], [15], [16]. However, these works have considered neither the possibility of installing other active resources such as ESSs nor the coupling of the ADNs' planning with their dispatchability. Indeed, the exploitation of ESS assets to achieve the ADN's dispatchability may affect the power flows within the network hosting high renewable generation capacities and thus impact the operation and planning decisions of the DSOs. Therefore, this paper aims at bridging this gap by developing a dedicated planning strategy that co-optimizes the investments associated with both line reinforcement and ESS deployment while taking into account the uncertainties of prosumption[3] to achieve ADNs dispatchability.

II. Literature Review

The existing literature has already proposed joint planning strategies considering ESSs and network reinforcement. The associated works can be grouped according to DSOs' operational objectives, namely: (i) minimization of grid losses [17], (ii) maximization of grid reliability [17]–[20], (iii) minimization of distributed generation (DG) curtailment [17] (iv)

[1]The European Union's regulatory directive is currently prohibiting DSOs' ownership of ESSs used in purpose of balancing and congestion management in order to prevent distortion of competitive market for energy storage [9].

[2]The hosting capacity of a power grid corresponds to the amount of loads and generation that can be hosted without violating any operational constraint.

[3]Prosumption is defined as the load consumption minus the locally generated power.

minimization of electricity and operation costs of both DG and ESSs [19]–[22], (v) minimization of maintenance costs [19], [20]. In addition to the above-listed operational objectives, controllable ESSs may also be used to procure flexibility services to the local distribution system, such as peak shaving [18], [21], [23] as well as ancillary services to the upper-level grid [23]. Furthermore, ESSs and DG may also be controlled with the objective of reducing carbon emissions of power generation [22]. Yet, to the best of the authors' knowledge, the objective of achieving ADNs dispatchability has not been addressed by the existing joint planning of ESSs and line reinforcement, and it is the aim of this paper.

Given that the system operation largely influences the ADN planning, evaluating the network's compliance with the grid constraints is indispensable for each investment decision made in the planning stage. In this regard, the operational characteristics of the network including active components should be modeled accurately to ensure the reliability of the planning solution [24]. The planning method proposed in [21] fully considered the AC power flow and associated grid constraints, making the embedded operation problem non-linear and non-convex. The problem is solved by employing particle swarm optimization, but high solution quality cannot be guaranteed by employing such a meta-heuristic solution approach.

Alternatively, the non-linearity of the AC-OPF model may be tackled by linear approximations of power flow equations and constraints. In this way, the planning problem was formulated as a mixed-integer linear programming (MILP) problem in [17]–[20]. The multi-stage joint planning model proposed in [18] considered replacing/adding lines while integrating ESSs for peak shaving and enhancing the power supply reliability. Kirchhoff's laws are used to linearize the voltage drop in the power flow formulation. However, the main drawback of linear OPF models lies in the approximation accuracy of physical quantities in the power flow as it depends on the operating point, possibly resulting in solutions characterized by a quality that can vary with the operating condition.

Another approach convexifies the AC-OPF model to a second-order cone programming (SOCP) problem [25]. The joint planning of line and DGs proposed in [26] utilized the SOCP model of power flow and grid constraints, and a stochastic programming planning problem is solved by employing commercial solvers. In [27], Haghighat et al. proposed a two-stage stochastic mixed-integer SOCP (MISOCP) model and its chance-constrained variant to make the problem more tractable. However, the stochastic prosumption was modeled with a load duration curve, making it difficult to accurately include the operational aspect of the ADN along with the prosumption changing with time. The SOCP model employed in [26], [27] neglected the presence of branch shunt elements and, as a consequence, the exactness of the solution cannot be guaranteed in case of reverse power flow and binding line ampacity and upper voltage-magnitude limits.

In this respect, this paper proposes a co-optimization method for the allocation of ESSs and lines reinforcement based on a scenario-based stochastic MISOCP model. Prediction uncertainties of seasonal prosumption are modeled through representative time-series prosumption scenarios. Grid operational constraints are described by the augmented relaxed OPF (AR-OPF) model, initially proposed in [28] and modified in [13]. In [28], Nick et al. proved that the AR-OPF outperforms the SOCP model proposed in [25] in terms of exactness of the solution especially in the case mentioned above. The AR-OPF model has been suitably modified in [13] for the specific problem of ADNs dispatchability achieved by the use of ESSs, while complying with the fundamental feature of guaranteeing the exactness of the OPF model. Hereafter, such a modified AR-OPF is referred to MAR-OPF model.

Along with binary and continuous decision variables representing ESSs investment decisions [13], in this paper the line reinforcement is modeled by incorporating binary and continuous decision variables associated with the line candidates for reinforcement and their conductors' size. The proposed planning framework is general enough to give the modeler the choice of planning options of ESSs and line reinforcement by quantitatively assessing the ESSs' influence on the network reinforcement. The line reinforcement is incorporated into the grid constraint associated with the line ampacity, while the corresponding change in the line parameters is considered within the ADN operation.

The Benders decomposition is widely used to reduce the computational complexity of large-scale optimization problems, such as planning problems. For instance, in [27], the planning problem is decomposed into two stages by employing the Benders decomposition methods. In the master problem, the decision variables associated with substation and capacitor investment are determined based on the system operation evaluation assessed through solving the subproblem. Likewise, the Benders decomposition is employed to tackle the ESS allocation problem in [13], while binary and continuous decision variables are assigned to the ESS location and the ESS capacity, respectively, and their optimal values are obtained together in the master problem. In this paper, to better tackle the increased complexity caused by the additional introduction of numerous binary variables associated with the line reinforcement, the planning problem is reformulated to employ the Benders decomposition separately to determine the site and size of the assets investment in sequential stages. This non-trivial structural change reduces the computation time for solving the planning problem while maintaining the optimality of the obtained solution. Consequently, it enables the scalable application of the proposed planning methodology to radial distribution networks of generic sizes.

To summarize, the contributions of the paper are given below.

1) A joint planning problem considering ESSs and line reinforcement is proposed to achieve ADNs dispatchability while ensuring sufficient hosting capacity for increasing stochastic prosumption.
2) The line reinforcement investment is suitably modeled along with corresponding adjustments on the network admittance matrix and the grid constraints in order to be incorporated in the MAR-OPF model.
3) The reformulation of the planning problem is proposed to determine the siting and sizing of the investment assets sequentially, thereby accelerating the convergence of the Benders decomposition algorithm.

The paper is organised as follows: in Section II, we introduce the structure of the optimization problem and explain the key parts. In Section III, the proposed problem and the associated solution are described. Section IV contains a detailed application example referring to the co-planning of ESSs and line reinforcement on a real ADNs. Finally, Section V concludes the paper discussing the main findings.

III. System description

The targeted network is assumed to have a radial topology. All the buses (excluding the slack bus) are connected to the upstream ones with only one line. Therefore, the bus and the

line connected upstream to each bus can be indicated with the same index, $l \in \mathcal{L}$. The joint optimal allocation of ESS and network reinforcement are determined based on the operation of the ADN over the planning time horizon Y. The load consumption is assumed to grow annually over the planning horizon with a constant rate r_g. The seasonal variation in the prosumption profile is represented by typical day-types indexed with $d \in \mathcal{D}$. The uncertainty of the prosumption power profile for day d and year $y \in \mathcal{Y}$ is modeled by scenarios indexed with $\phi \in \Phi_{dy}$, where Φ_{dy} is defined $\forall d \in \mathcal{D}$ and $\forall y \in \mathcal{Y}$. The probability associated to the occurrence of each scenario is given by λ_ϕ. In each day-type, the active power through GCP of ADN (assigned with the bus number $l=1$) is dispatched following a day-ahead determined daily dispatch plan ($DP_{tdy}, \forall t \in \mathcal{T} := \{1, \ldots, T\}$) derived thanks to the support of a forecasting tool[4]. T is the number of dispatch intervals, and t is the index of time intervals separated by a constant timestep Δt. Multiple operational objectives are taken into account: achieving the dispatchability of the targeted ADN while minimizing the grid losses and ensuring the feasibility of the ADN operation. ESSs and line reinforcement are the assets to be planned to cope with this problem.

Each bus of the ADN is assumed to have non-dispatchable aggregated complex power prosumption where the stochasticity of the prosumption is modeled by a set of scenarios ($s_{l\phi t} = p_{l\phi t} + j q_{l\phi t}$) defined at each time interval. The objective of the dispatch problem is to make the active power flow through the ADN GCP in all scenarios ($P_{1\phi t}$) follow the daily dispatch plan over the operation horizon T by minimizing the observed active dispatch error, thereby avoiding a corresponding imbalance penalty. In this regard, ESSs are allocated within the ADN (*i.e.*, $U_l = 1$, where $U_l \in \{0, 1\}$ is the ESS installation status at bus l with the ESS energy capacity of C_l and the power rating of R_l). Their active power ($p^E_{l\phi t}$) is dispatched to compensate for the gap between the dispatch plan and active power flow of scenario ϕ at time interval t at the GCP. The reactive power ($q^E_{l\phi t}$) is dispatched to support the reactive power flows to keep the system operating point within all imposed constraints.

Meanwhile, the large amount of stochastic distributed generation increases the risk of line congestion and reduces the power supply reliability. In this respect, we determine the lines to be upgraded among the existing ones (*i.e.*, $X_l = 1$, where $X_l \in \{0, 1\}$ indicates whether to upgrade the line l). The required change in line ampacity is decided to minimize the load curtailment, which serves as the reliability indicator of the power supply of the ADN loads.

A specific complexity of the targeted planning problem is associated with the fact that the change of line conductors produces a change of the line parameters. As the line ampacity increases, the line resistance and the reactance decrease, while the line susceptance increases. The dependence of the line parameters on its ampacity is modeled through a linear fitting for line reactance and susceptance and a hyperbolic fitting for the line resistance. The sensitivity coefficients of the line parameters computed from the fitted curves are introduced within the OPF to accurately model the effect of line reinforcement on the line parameters (see Sec. V for the graphs of the line parameters). In view of the above, the proposed ESS allocation and line reinforcement problem can be seen as a two-stage decision process: the first stage deals with the binary decision variables on the location of the ESS (U_l), the lines to be upgraded (X_l) and the continuous decision variables on the capacity of the ESSs energy reservoirs (C_l), their power rating (R_l), and the line ampacity (A_l), whereas the second stage deals with daily dispatch problems, determining the decision variables on the ESSs active and reactive power for all operating scenarios.

[4]In the rest of the paper, we assume a suitable forecasting tool to be available and with known prediction uncertainties.

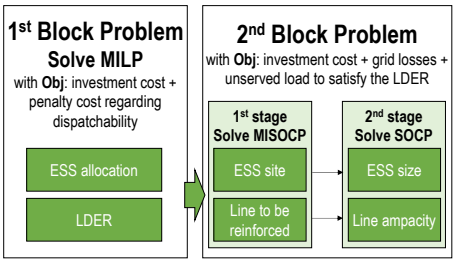

Fig. 1. Solution algorithm overview of the proposed method.

IV. Problem Formulation

The objective of the problem is to maximize the DSO benefits associated to the co-optimization of ESSs and line reinforcement in a given ADN. The operational objective is to maintain a sufficient level of the ADN dispatchability while complying with the network constraints in a (potentially) highly congested network due to significant penetration of uncontrollable DG units and load consumption. The planning problem is decomposed in two blocks. In the 1st block, the economical benefits/penalties associated with the network dispatchability are obtained by quantifying the trade-off between the ESSs allocation costs vs. the avoidance on the power dispatch imbalance penalties. In the 2nd block, the ESSs allocation and the line reinforcement investment are determined by employing the AR-OPF model to satisfy a dispatch error level obtained from the 1st block, while complying with the network operating constraints. Such a two-block problem structure is essential to abide by the pre-requisite condition for the AR-OPF model to guarantee exactness [13]. In view of its complexity, the 2nd block of the problem is further decomposed in two stages to separately determine the solutions of the binary and continuous variables regarding the investment decisions. In the 1st stage, the sites for the ESSs and line reinforcement are determined. Then, with these sites, the values of the continuous variables are determined by the 2nd stage. The algorithm of the proposed approach is illustrated in Fig. 1. All the variables in this section with subscript l, ϕ, t, d, y are defined for $l \in \mathcal{L}$, $\phi \in \Phi_{dy}$, $t \in \mathcal{T}$, $d \in \mathcal{D}$, $y \in \mathcal{Y}$.

A. The 1st block problem

In the 1st block, the planning problem is modeled as a MILP one. It determines the optimal ESSs allocation and the grid dispatchability level by evaluating the operational benefit of ESSs for all operating scenarios. The problem minimizes the investment and total penalty costs over the planning horizon while employing the linear Distflow model. In this OPF model, the shunt elements of the lines are taken into account[5], whereas the grid losses and the line ampacity constraints are ignored.

1) Modeling of the ESSs investment: the ESSs investment is modeled through (1a)-(1c). Power ratings and energy capacities are governed by geographical restriction related to the candidate location for ESS investment. (1a) models the minimum and maximum of possible ESS power rating

[5]In this way, the reactive power generated by the shunt impedance of the line is taken into account in the nodal voltage constraints.

capacity while (1b) models the minimum and maximum of possible ESS energy reservoir capacity at bus l, respectively. CR^{max} is the maximum value for the rate at which ESS is discharged relatively to its maximum energy capacity. The power rating and energy reservoir is determined considering this relationship as shown in (1c). The ESS investment cost is denoted as IC_E and defined by (1d), where ic_E^f, ic_E^p, ic_E^e are cost parameters for the ESS installation, power rating, and energy reservoir, respectively.

$$R_l^{min}U_l \leq R_l \leq R_l^{max}U_l, \quad \forall l \tag{1a}$$
$$C_l^{min}U_l \leq C_l \leq C_l^{max}U_l, \quad \forall l \tag{1b}$$
$$\Delta t \cdot R_l \leq CR^{max} \cdot C_l, \quad \forall l \tag{1c}$$
$$IC_E = \sum_{l\in\mathcal{L}} (ic_E^f U_l + ic_E^p R_l + ic_E^e C_l) \tag{1d}$$

2) Modeling of the ESS operation: the ESS power ($s_{l\phi t}^E = p_{l\phi t}^E + jq_{l\phi t}^E$) is governed by the operational constraints of ideal ESS as shown in (2a)-(2f). $E_{l\phi t}^E$ is the state of energy (SoE) of ESS installed at bus l for time t and scenario ϕ. The typical circular capability curve defined by the maximum complex power of a given ESS is linearized and modeled by the vectors of coefficient parameters α_l, β_l, κ_l as shown in (2a) [29]. The SoE changes with the charge/discharge power of the ESS at every time interval, as described in (2b). According to (2c), the SoE should be within the minimum and maximum allowed SoE level. As indicated in (2d), the initial SOE is set as $E_{ini} \cdot 100(\%)$ of the installed energy reservoir capacity for each day-type (in this paper, the value for E_{ini} is set to 0.5). The final SoE is set to be within $\pm(\Delta^f \cdot 100)\%$ of the given initial SoE as in (2e) to assure the continuous operation over consecutive days (the value of Δ^f is set to 0.1). To minimize the ageing linked to the ESS daily cycling, as shown in (2f), the energy exchange of ESS is kept within a threshold obtained from the battery ageing-aware control strategy proposed in [30]. N_c is the allowed number of cycles per day and ω is a positive parameter that depends on $p_{l\phi t}^E$. The ideal ESSs operation is implemented in the 1st block problem and the 1st stage of the 2nd block problem. In the following 2nd stage problem (*i.e.*, when sizing the ESS capacity), however, the ESSs charging/discharging efficiency is considered by adding a virtual resistive line adjacent to the node with ESS[6] [31].

$$\alpha_l p_{l\phi t}^E + \beta_l q_{l\phi t}^E \leqslant \kappa_l R_l, \quad \forall l, \forall \phi, \forall t \tag{2a}$$
$$E_{l\phi(t+1)}^E = E_{l\phi t}^E + \Delta t \cdot p_{l\phi t}^E, \quad \forall l, \forall \phi, \forall t \tag{2b}$$
$$E^{min}C_l \leq E_{l\phi t}^E \leq E^{max}C_l, \quad \forall l, \forall \phi, \forall t \tag{2c}$$
$$E_{l\phi(1)}^E = E_{ini}C_l, \quad \forall l, \forall \phi \tag{2d}$$
$$E_{l\phi(1)}^E - \Delta^f C_l \leq E_{l\phi(T+1)}^E \leq E_{l\phi(1)}^E + \Delta^f C_l, \quad \forall l, \forall \phi, \forall t \tag{2e}$$
$$\frac{\Delta t}{2 \cdot 1h} \sum_{t=1}^{T} |\omega p_{l\phi t}^E| \leq N_c C_l, \quad \forall l, \forall \phi, \forall t \tag{2f}$$

For the sake of brevity, (2a)-(2f) are indicated by $\Xi(\eta) \geq 0$ where $\eta = \{p^E, q^E, E^E, R, C\}$ is the set of variables. The notation without subscript corresponds to the vectors of variables for all buses/lines, all timesteps and all scenarios.

3) Modeling of the ADN operation: $p_{l\phi t}$ and $q_{l\phi t}$ represent the complex prosumption for bus l, scenario ϕ, and time t. $\tilde{p}_{ltdy}$ is the active prosumption prediction for bus l, time t, day d, and year y respectively. The prosumption scenarios are generated based on the assumption that the prosumption follows a normal distribution. Therefore, the prosumption prediction at node l ($\tilde{p}_{ltdy}$) is equivalent to the average of the prosumption over the scenarios. The dispatch plan (DP_{tdy}) follows the prosumption prediction, as modeled by (3a). As shown in (3b), the aggregated prosumption deviation from the prosumption prediction is compensated by the ESS power, and thus $\epsilon_{l\phi t}$ represents the residual dispatch error that cannot be covered at bus l, scenario ϕ, and time t. The upstream bus of bus l is noted as $\bar{l}$. $\mathbf{G}$ is the adjacency matrix of the network, where $\mathbf{G}_{kl}$ is defined for $k, l \in \mathcal{L}$ and $\mathbf{G}_{kl}=1$ if $k=\bar{l}$ or 0 if not. $S_{l\phi t}^t = P_{l\phi t}^t + jQ_{l\phi t}^t$ indicates the complex power injected into line l from node $\bar{l}$ at scenario ϕ and time t. $S_{l\phi t}^b = P_{l\phi t}^b + jQ_{l\phi t}^b$ is the complex power injected into node l from line l. $v_{\bar{l}\phi t}$ and $v_{l\phi t}$ represents the squared nodal voltages at node $\bar{l}$ and l, respectively. b_l indicates the shunt susceptance of line l. v^{min} and v^{max} represent lower and upper limit of squared nodal voltage, respectively. In the lossless Distflow model, the power flows from the sending end to line l and from line l to the receiving end including the ESS power are expressed via (3c)-(3e), respectively. The active power at the sending/receiving end for line l are determined by (3c), while the reactive power at the sending/receiving for line l are given by (3d)/(3e), respectively. Equation (3f)[7] computes the nodal voltage, which is governed by the voltage constraint (3g).

$$DP_{tdy} = \sum_{l\in\mathcal{L}} \tilde{p}_{ltdy}, \quad \forall t, \forall d, \forall y \tag{3a}$$
$$DP_{tdy} - \sum_{l\in L} p_{l\phi t} = \sum_{l\in\mathcal{L}} (\epsilon_{l\phi t} + p_{l\phi t}^E), \quad \forall \phi, \forall t, \forall d, \forall y \tag{3b}$$
$$P_{l\phi t}^t = P_{l\phi t}^b = p_{l\phi t} + p_{l\phi t}^E + \sum_{m\in\mathcal{L}} \mathbf{G}_{lm} P_{l\phi t}^t, \quad \forall l, \forall \phi, \forall t \tag{3c}$$
$$Q_{l\phi t}^t = q_{l\phi t} + q_{l\phi t}^E + \sum_{m\in\mathcal{L}} \mathbf{G}_{lm} Q_{l\phi t}^t - (v_{\bar{l}\phi t} + v_{l\phi t}) b_l, \forall l, \forall \phi, \forall t \tag{3d}$$
$$Q_{l\phi t}^b = q_{l\phi t} + q_{l\phi t}^E + \sum_{m\in\mathcal{L}} \mathbf{G}_{lm} Q_{l\phi t}^t, \quad \forall l, \forall \phi, \forall t \tag{3e}$$
$$v_{l\phi t} = v_{\bar{l}\phi t} - 2\Re\Big(\bar{z}_l (S_{l\phi t}^t + j v_{\bar{l}\phi t} b_l)\Big), \quad \forall l, \forall \phi, \forall t \tag{3f}$$
$$v^{min} \leq v_{l\phi t} \leq v^{max}, \quad \forall l, \forall \phi, \forall t \tag{3g}$$

The optimization problem of the 1st block is given below. The objective function is defined to minimize the ESSs investment cost (IC_E) and the annual penalty cost regarding the uncovered dispatch error over the planning horizon. The penalty cost of day d and year y is the uncovered dispatch error over the operating scenarios for day d and year y multiplied by ω_d, which is the cost coefficient for the imbalance. N_{dy} is the number of days in year y that have the same prosumption profile as that of typical day d. r_i is the discount rate. Ω_1 and Ω_2 represents the set of control variables in the first and second stage decision process, respectively (See Sec. III.)

$$\min_{\Omega_1,\Omega_2} IC_E + \sum_{y\in\mathcal{Y}} \frac{1}{(1+r_i)^y} \sum_{d\in\mathcal{D}} N_{dy} w_d \sum_{t\in\mathcal{T}} \sum_{\phi\in\Phi_{dy}} \lambda_\phi \Big| \sum_{l\in\mathcal{L}} \epsilon_{l\phi t} \Big| \tag{4}$$

subject to
$$(1), (3), \tag{5}$$
$$\Xi_{dy}(\eta) \geq 0, \forall d, \forall y \tag{6}$$

[6]The resistances are updated in proportion to the ESS capacity using the reference value in [31].

[7]$\Re(.)$ represents the real part of a complex number and $\bar{z}_l$ represents the complex conjugate of z_l.

By solving this problem, the optimal allocation of ESSs along with the dispatch plan are both obtained, and the daily leftover dispatch error rate (LDER) is calculated by (7)[8] for each day with index $d \in \mathcal{D}$ and all years with index $y \in \mathcal{Y}$.

$$\theta_{\phi t} = \frac{|\sum_{l \in \mathcal{L}} \epsilon^*_{l\phi t}|}{|\sum_{l \in \mathcal{L}} \Delta p_{l\phi t}|}, \quad \forall \phi, \forall t \tag{7}$$

B. 2nd block problem

The objective of the 2nd block problem is to determine the ESS allocation as well as the line reinforcement scheme in order to minimize the load curtailment and the grid losses. The dispatchability level is incorporated into the 2nd block problem as a constraint governed by the dispatchability index LDER. The investment decision is optimized based on the investment cost for the ESS allocation and the line reinforcement given by (8). ic_l^r is the fixed cost parameter of the line reinforcement for line l. ρ_l is the line length of l. The line reinforcement cost, modeled by (9), consists of two parts: fixed cost, which is invariant with the conductor size and accounts for the construction, labor, etc., and the conductor cost, which varies with line ampacity and line length. Based on the line cost data from [32], the line cost per kilometer is modeled as a quadratic function of the line ampacity, where $\delta_2, \delta_1, \delta_0$ are the coefficients for the squared, linear and constant terms in the quadratic function.

$$IC = IC_E + IC_L \tag{8}$$

$$IC_L = \sum_{l \in \mathcal{L}} (ic_l^r X_l + \rho_l(\delta_2 A_l^2 + \delta_1 A_l + \delta_0 X_l)) \tag{9}$$

The system operating condition during the operation horizon with each set of investment decisions is evaluated through solving the daily convexified AC-OPF problem, or MAR-OPF problem. Therefore, the 2nd block problem is formulated as a MISOCP problem. Regarding the investment decisions, we tackle binary (U, X) and continuous investment decisions (R, C, A) separately in the 1st stage and the 2nd stage problems, by formulating them as a MISOCP problem and a SOCP problem, respectively. The approach is depicted in the block diagram shown in Fig. 2. We apply the Benders decomposition

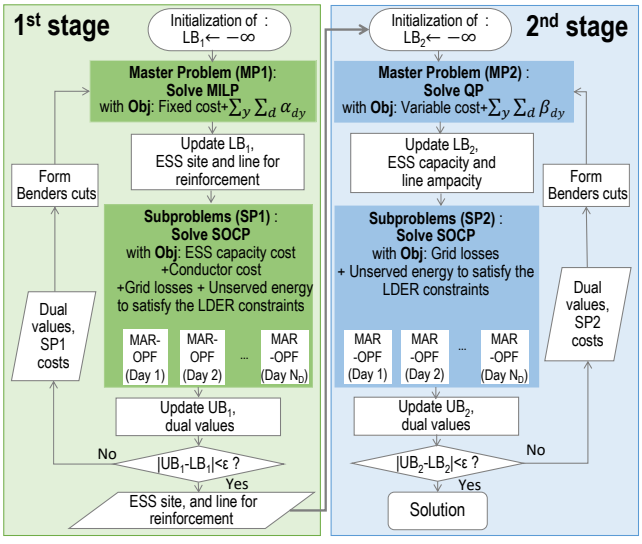

Fig. 2. Detailed structure of the 2nd block problem.

to both stages obtaining a master problem and several parallel subproblems. In the 1st stage, the master problem determines the site of the ESS allocation and the line reinforcement. Then, each subproblem, which is represented by a daily OPF problem, determines the ESS capacity and the upgraded line ampacity specific to each day-type and year to minimize the unserved load and comply with the dispatchability constraint. The unserved load takes values to ensure the feasibility of the subproblem regardless of the investment decision. Once the convergence of the Benders decomposition is reached, the binary solutions of the 1st stage are passed to the 2nd stage problem. The master problem considers the ESS capacity for the buses chosen to have ESSs investment and the line ampacity for the lines identified to be reinforced. The subproblem deals with the fitness evaluation of the determined allocations in terms of the same operational requirement and objectives as in the 1st stage subproblem.

1) Modified Augmented Relaxed Optimal power flow: In this section, the MAR-OPF model including ESS assets for a radial power network is described. As only a brief description of the power flow equations is provided, readers are referred to [28] for detailed explanation.

a) Power flow equations: the feasibility of system operation is assessed by the unserved energy due to load curtailment. As indicated in (10a), we introduce positive and negative unserved active and reactive load terms ($up_l^+ - up_l^-$ and $uq_l^+ - uq_l^-$). Therefore, $s'_l = p'_l + jq'_l$ can be described as complex prosumption required for the feasible operation of the considered ADN. Henceforth, s_l is replaced with s'_l in the power flow equations.

All the variables and parameters shared in the Distflow model and the AR-OPF model are already explained in Sec. IV-A3. One of the essential differences between the two models is the representation of current and line losses. Let f_l be the square of the longitudinal current through line l which produces grid losses through the line longitudinal impedance $z_l = r_l + jx_l$ of a Π two-port model. The branch power flow equations including ESS power dispatch at the sending end and the receiving end of line l, squared nodal voltage magnitude, and line current through longitudinal element are described for the set of state variables ((10b)-(10e)), respectively. As shown by (10e), the equations for the longitudinal line current are relaxed to second order cone constraints.

$$p'_l + jq'_l = (p_l + up_l^+ - up_l^-) + j(q_l + uq_l^+ - uq_l^-), \quad \forall l \tag{10a}$$

$$S_l^t = s'_l + s_l^E + \sum_{m \in \mathcal{L}} \mathbf{G}_{lm} S_l^t + z_l f_l - j(v_{\bar{l}} + v_l) b_l, \quad \forall l \tag{10b}$$

$$S_l^b = s'_l + \sum_{m \in \mathcal{L}} \mathbf{G}_{lm} S_l^t, \quad \forall l \tag{10c}$$

$$v_l = v_{\bar{l}} - 2\Re\left(\bar{z}_l \left(S_l^t + jv_{\bar{l}} b_l\right)\right) + |z_l|^2 f_l, \quad \forall l \tag{10d}$$

$$f_l v_{\bar{l}} \geq |S_l^t + jv_{\bar{l}} b_l|^2, \quad \forall l \tag{10e}$$

The contribution of the AR-OPF is to ensure the exactness of the solution of convexified OPF by introducing auxiliary variables $\bar{f}_l$, $\bar{S}_l = \bar{P}_l + j\bar{Q}_l$, $\bar{v}_l$ and $\hat{S}_l = \hat{P}_l + j\hat{Q}_l$, which stand for the upper bounds for squared longitudinal current, complex power, squared nodal voltage and lower bounds for the complex power of line l, respectively. I_l^t and I_l^b are the square of the line current injected into line l from node $\bar{l}$ and from line l into bus l, respectively. I_l^{max} indicates the ampacity value of line l. P_l^{max} and Q_l^{max} are the upper limits of active and reactive power flows for line l, respectively. The lower bound branch power flow equations from the sending and the receiving end of line l are given by (11a) and (11b), followed by (11c), which defines the squared upper bound nodal voltage magnitude. The branch upper bound power flow equations at the sending and the receiving end of line l are given by (11d)

[8] $(.)^*$ represents the optimal value of the variable.

and (11e). Eqs. (11f) and (11g) express that the upper bound of the current f_l is decided by the maximum of absolute complex power flow from both sides of line l. Eq. (11h) is imposed on upper bound power variables for the exactness of the solution. The voltage constraint is modeled as (11i). The ampacity constraint from the sending end and the receiving end are modeled as in (11j)-(11l).

$$\hat{S}_l^t = s_l' + s_l^E + \sum_{m\in\mathcal{L}} \mathbf{G}_{lm}\hat{S}_l^t - j(\bar{v}_{\bar{l}}+\bar{v}_l)b_l, \quad \forall l \quad (11a)$$

$$\hat{S}_l^b = s_l' + s_l^E + \sum_{m\in\mathcal{L}} \mathbf{G}_{lm}\hat{S}_l^t, \quad \forall l \quad (11b)$$

$$\bar{v}_l = \bar{v}_{\bar{l}} - 2\Re\Big(\bar{z}_l(\hat{S}_l^t + j\bar{v}_{\bar{l}}b_l)\Big), \quad \forall l \quad (11c)$$

$$\bar{S}_l^t = s_l' + s_l^E + \sum_{m\in\mathcal{L}} \mathbf{G}_{lm}\bar{S}_l^t + z_l f_l - j(v_{\bar{l}}+v_l)b_l, \quad \forall l \quad (11d)$$

$$\bar{S}_l^b = s_l' + s_l^E + \sum_{m\in\mathcal{L}} \mathbf{G}_{lm}\bar{S}_l^t, \quad \forall l \quad (11e)$$

$$\begin{aligned}&\bar{f}_l v_l \geq |\max\{|\hat{P}_l^b|, |\bar{P}_l^b|\}|^2 \\ &+|\max\{|\hat{Q}_l^b - j\bar{v}_l b_l|, |\bar{Q}_l^b - j v_l b_l|\}|^2, \quad \forall l\end{aligned} \quad (11f)$$

$$\begin{aligned}&\bar{f}_l v_{\bar{l}} \geq |\max\{|\hat{P}_l^t|, |\bar{P}_l^t|\}|^2 \\ &+|\max\{|\hat{Q}_l^t + j\bar{v}_{\bar{l}} b_l|, |\bar{Q}_l^t + j v_{\bar{l}} b_l|\}|^2, \quad \forall l\end{aligned} \quad (11g)$$

$$\bar{P}_l^t \leq P_l^{max},\ \bar{Q}_l^t \leq Q_l^{max}, \quad \forall l \quad (11h)$$

$$v^{min} \leq v_l,\ \bar{v}_l \leq v^{max}, \quad \forall l \quad (11i)$$

$$I_l^t v_{\bar{l}} \geq |\max\{|\hat{P}_l^t|, |\bar{P}_l^t|\}|^2 + |\max\{|\hat{Q}_l^t|, |\bar{Q}_l^t|\}|^2, \quad \forall l \quad (11j)$$

$$I_l^b v_l \geq |\max\{|\hat{P}_l^b|, |\bar{P}_l^b|\}|^2 + |\max\{|\hat{Q}_l^b|, |\bar{Q}_l^b|\}|^2, \forall l \quad (11k)$$

$$I_l^t \leq (I_l^{max})^2,\ I_l^b \leq (I_l^{max})^2, \quad \forall l \quad (11l)$$

For the sake of readability, the equations regarding the AR-OPF model are grouped and represented by $\Theta(\varphi)\geq 0$ where $\varphi = \{S^t, v, f, \hat{S}^t, \bar{v}, \bar{f}, \bar{S}^t, s', s^E, \epsilon\}$ is the set of variables. The notation without subscript corresponds to the vector of variables for all buses/lines.

b) Defining the dispatch error: Several modifications are made to the AR-OPF model to consider the ADN operation while achieving the desired level of dispatchability of the distribution feeder. Any further explanation of the formulation of the modified AR-OPF (MAR-OPF) model can be found in [13]. The prosumption scenarios can be written as the sum of the prosumption prediction and the deviation of prosumption $\Delta p'_{l\phi t}$ given by (12a). In order to include the grid losses into the dispatch error calculation, the grid losses corresponding to the prosumption prediction are expressed by the losses prediction $r_l\tilde{f}_{ltdy}$ and the prediction error $r_l\Delta f_{l\phi t}$ given by (12b). In this context, the *dispatch error* with no dispatchable resources in ADN is formally defined as the total deviation of the prosumption and the line losses over the buses/lines as given by the left-hand side of (12c). The ESSs active power dispatch compensates for the total deviation of power from the dispatch plan. To improve the accuracy of the grid losses calculation, two slack variables $\gamma_{\phi t}^m$ and $\zeta_{\phi t}^m$ ($m\in\mathcal{M}_1$ for 1st stage and $m\in\mathcal{M}_2$ for 2nd stage problem), which approximate the grid losses deviation for scenario ϕ and time t, are introduced. The approximated grid losses deviation is updated as shown in (12d) throughout the iterative algorithm used to solve the MAR-OPF problem. The iterative loop terminates when $\zeta_{\phi t}^m$ becomes lower than the tolerance value. (12e) indicates that the residual dispatch error should comply with the defined dispatchability level index, or LDER ($\theta_{\phi t}$).

$$p'_{l\phi t} = \tilde{p'}_{ltdy} - \Delta p'_{l\phi t}, \quad \forall l, \forall\phi, \forall t \quad (12a)$$

$$r_l f_{l\phi t} = r_l \tilde{f}_{ltdy} - r_l \Delta f_{l\phi t}, \quad \forall l, \forall\phi, \forall t \quad (12b)$$

$$\sum_{l\in\mathcal{L}}(\Delta p'_{l\phi t} + r_l\Delta f_{l\phi t}) = \sum_{l\in\mathcal{L}}(\epsilon_{l\phi t} + p_{l\phi t}^E) + \zeta_{\phi t}^m, \ \forall\phi, \forall t \quad (12c)$$

$$\sum_{l\in\mathcal{L}} \Delta p'_{l\phi t} + (\gamma_{\phi t}^m + \zeta_{\phi t}^{*m-1}) = \sum_{l\in\mathcal{L}}(\epsilon_{l\phi t} + p_{l\phi t}^E), \quad \forall\phi, \forall t \quad (12d)$$

$$|\sum_{l\in\mathcal{L}} \epsilon_{l\phi t}| \leq \theta_{\phi t} |\sum_{l\in\mathcal{L}} \Delta p_{l\phi t}|, \quad \forall\phi, \forall t \quad (12e)$$

2) 1st stage - Determination of the ESS site and line for reinforcement: the problem structure of the 1st stage problem is illustrated on the left side of Fig. 2. As already mentioned, the nodes for ESS and line for reinforcement are determined in the master problem. The optimal ESSs size and change of lines specific to the each day-type, and resulting operational benefit is evaluated within each subproblem. As the goal of this stage is to determine the best solution for the set of binary variables, the different ESS and line conductor sizes determined for each day-type are not the final solutions.

a) Master problem: the formulation of the master problem is given in (13). The master problem only deals with the cost determined by binary variables regarding the nodes for ESS installation and line reinforcement. The objective function value of the master problem is computed by summing the fixed investment cost plus a portion of the conductor cost associated with the binary variables, and the lower approximation of the expected subproblem costs. α_{dy} represents the subproblem cost for day-type d for year y. It is initially bounded by $\underline{\alpha}$, which is the parameter given as the lower bound for the subproblem cost. $n\in\mathcal{N}_1$ is the index of the Benders iterations of the 1st stage problem. In every nth iteration, the Benders multi cuts represented by $\Gamma_{dy}^{(n)}$, $\forall d\in\mathcal{D}, y\in\mathcal{Y}$, are added, as shown in (13c). The lower bound of the total cost, so-called LB_1, is the optimal objective value of the master problem (*i.e.*, $LB_1 = MC^{1*}$).

$$\min_{U,X,\alpha}: MC^1 = \sum_l ic_E^f U_l + \sum_l (ic_l^r + \rho_l\delta_0)X_l + \sum_y\sum_d \alpha_{dy} \quad (13a)$$

$$\text{subject to:} \quad \alpha_{dy} \geq \underline{\alpha}, \quad \forall d, \forall y \quad (13b)$$

$$\alpha_{dy} \geq \Gamma_{dy}^{(n)}, \quad \forall d, \forall y, \forall n. \quad (13c)$$

b) Subproblem: in the subproblem associated with day-type d and year y, a daily MAR-OPF model, with the time-step discretization Δt, sizes the ESSs capacity and lines ampacity while evaluating the investment plan based on its operational advantages on the system conditions. The optimization problem is modeled by the MAR-OPF as discussed in Sec. IV-B1. On top of that, the constraints modeling the line ampacity and the ESS capacity are included in the subproblem. The possible range of ampacity is modeled by (14a), while A^{min}/A^{max} represent minimum/maximum possible line capacity, respectively. However, as the line ampacity constraint is given with the the squared current variable (see (11l)), we need to model the squared ampacity to impose the ampacity constraints on the current variable. The approximated value of the squared ampacity ($L(A_l^2)$) is used. The piecewise linearization technique is employed to approximate the squared ampacity as shown in (14c), while k is the step index and K_1 is the number of discretization steps. The possible range of squared ampacity is modeled as (14b). The ampacity constraint is modified

accordingly from (11l) to (14d), and (14e). The variables regarding the line for reinforcement and the squared ampacity are introduced in the right-hand side of (14d) and (14e).

$$A^{min}X_l \le A_l \le A^{max}X_l, \qquad \forall l \tag{14a}$$
$$(A^{min})^2 X_l \le L(A_l^2) \le (A^{max})^2 X_l, \qquad \forall l \tag{14b}$$
$$L(A_l^2) \ge a_k A_l + b_k, \quad \forall k \in \{1,...,K_1\}, \forall l \tag{14c}$$
$$0 \le I_l^t \le (1-X_l)\cdot (I_l^{max})^2 + L(A_l^2), \qquad \forall l \tag{14d}$$
$$0 \le I_l^b \le (1-X_l)\cdot (I_l^{max})^2 + L(A_l^2), \qquad \forall l \tag{14e}$$

By incorporating the constraints related to the line reinforcement described above and the ESSs investment constraints (see (1)) into the OPF constraints described in Sec. IV-B1, we can define the subproblems of the 1st stage as follows. The objective function of the subproblem is defined by (15a). It consists of the capacity cost of the ESS energy reservoir and power rating, as well as the conductor cost with respect to the upgraded ampacity caused by the line reinforcement. Also, it includes the operational cost, which consists of grid losses cost and the unserved energy cost. Eq. (15e) describes how the ESS location and line to be reinforced are fixed to the optimal solution values of the master problem. τ_{ldy} and χ_{ldy} are the duals of constraints related to the fixed ESSs locations and the lines for reinforcement.

$$\begin{aligned}\min_{\forall C,R,A,\varphi,\eta,UL}: SC_{dy}^1 = {} & \frac{N_{dy}}{(1+r_i)^y}\sum_{t\in\mathcal{T}}\sum_{\phi\in\Phi_{dy}}\lambda_\phi\Big(w_l\sum_{l\in\mathcal{L}} r_l f_{l\phi t} \\ & + w_u\sum_{l\in\mathcal{L}}(up_{l\phi t}^{+}+up_{l\phi t}^{-}+uq_{l\phi t}^{+}+uq_{l\phi t}^{-})\Big) \\ & + \frac{N_{dy}}{365*Y}\sum_{l\in\mathcal{L}}(ic_E^e C_l + ic_E^p R_l) \\ & + \frac{N_{dy}}{365*Y}\sum_{l\in\mathcal{L}}\rho_l(\delta_2 L(A_l^2)+\delta_1 A_l)\end{aligned} \tag{15a}$$

$$\text{subject to: } (1),(12),(14), \tag{15b}$$
$$\Theta(\varphi_{\phi t}) \ge 0, \qquad \forall \phi, \forall t \tag{15c}$$
$$\Xi(\eta_{\phi t}) \ge 0, \qquad \forall \phi, \forall t \tag{15d}$$
$$U_{ldy}=U_l^* : \tau_{ldy}, \;\; X_{ldy}=X_l^* : \chi_{ldy}, \;\; \forall l, \forall d, \forall y \tag{15e}$$

where $\varphi=\{S^t, v, f, \hat{S}^t, \bar{v}, \bar{f}, \bar{S}^t, s', s^E, \epsilon\}$ is the set of variables of MAR-OPF, and $UL=\{up^+, up^-, uq^+, uq^-\}$ is the set of variables related to the unserved load. w_l and w_u are the weight coefficients associated with the grid losses minimization and unserved load, respectively.

$$\begin{aligned}\Gamma_{dy}^{(n)} = \big[SC_{dy}^{1*} - \sum_{l\in\mathcal{L}}(\tau_{ldy}(U_l - U_l^*) \\ + \chi_{ldy}(X_l - X_l^*))\big], \forall d, \forall y, \forall n\end{aligned} \tag{16}$$

The Benders multi cuts for the master problem for the next iteration are built with the dual variables and the objective value of the subproblem as shown in (16). The upper bound of the total planning cost, or UB_1, is calculated summing the optimal investment cost and the subproblem costs (*i.e.*, $UB_1 = \sum_l ic_E^f U_l^* + \sum_l (ic_l^r + \rho_l \delta_0) X_l^* + \sum_{y\in\mathcal{Y}}\sum_{d\in\mathcal{D}} SC_{dy}^{1*}$).

3) 2nd stage - Determination of the ESSs size and reinforced lines ampacity:

a) Master problem: In the 2nd stage of the 1st block problem, based on the site for the ESS allocation and line reinforcement obtained from the 1st stage problem, we solve another optimization problem using the Benders decomposition to determine the optimal size of the ESS capacity and the line ampacity. Eq.(17) shows the total investment cost, while expressing the updated ampacity (A_l) as the sum of original ampacity (I_l^{max}) and the change of ampacity (ΔA_l). The possible range for the change of ampacity is given by (18c). The 2nd stage master problem is modeled only with continuous variables, keeping the installation status (U_l, X_l) fixed to the 1st stage solution (U_l^*, X_l^*). Therefore, the variable parts of the ESS investment cost (the part associated with energy reservoir and power rating) and the conductor cost (the part associated with the ampacity change) are only included in the objective of the master problem. The anticipated subproblem cost is approximated by β_{dy}. Starting from lower bound subproblem cost value $\underline{\beta}$, β_{dy} is updated by the Benders cuts $\Psi_{dy}^{(n)}$ defined for $\forall d \in \mathcal{D}$, $\forall y \in \mathcal{Y}$, $\forall n \in \mathcal{N}_2$, where $\mathcal{N}_2$ is the Benders iterations of the 2nd stage problem as given by (18d). The lower bound of the 2nd stage cost, LB_2, is the optimal objective value of the master problem (*i.e.*, $LB_2 = MC^{2*}$).

$$\begin{aligned}IC = {} & \sum_{l\in\mathcal{L}}\Big(ic_E^f U_l + ic_E^e C_l + ic_E^p R_l\Big) \\ & + \sum_{l\in\mathcal{L}}\Big(ic_l^r + \rho_l\big(\delta_2(I_l^{max}+\Delta A_l)^2 + \delta_1(I_l^{max}+\Delta A_l)+\delta_0\big)\Big)\cdot X_l\end{aligned} \tag{17}$$

$$\begin{aligned}\min_{\forall C,R,\Delta A,\beta}: MC^2 = {} & \sum_{l\in\mathcal{L}}(ic_E^e C_l + ic_E^p R_l) \\ & + \sum_{l\in\mathcal{L}}\rho_l(\delta_2(\Delta A_l)^2 + (2\delta_2 I_l^{max}+\delta_1)\Delta A_l) \\ & + \sum_y\sum_d \beta_{dy}\end{aligned} \tag{18a}$$

$$\text{subject to: } (1a)-(1c), \tag{18b}$$
$$0 \le \Delta A_l \le \Delta A^{max}, \qquad \forall l \tag{18c}$$
$$\beta_{dy} \ge \underline{\beta}, \;\; \beta_{dy} \ge \Psi_{dy}^{(n)}, \qquad \forall d, \forall y, \forall n \tag{18d}$$

b) Subproblem: The subproblem of the 2nd stage evaluates the system operational condition under the investment decision given by the master problem. The optimization problem is defined with the similar set of operating constraints as in the subproblem of the 1st stage. The squared change of line's ampacity is modeled through piecewise linearzation as shown in (19c), while the number of discretization steps (K_2) can be very small as the optimal value of the ampacity is already given from the master problem solution as shown in (19f). The changed ampacity limits are expressed as (19d) and (19e). As shown in (19a), the objective function is to minimize the total grid losses and unserved load to satisfy the LDER constraint, and the operation period spans all days grouped into each day-type over the planning horizon.

$$\begin{aligned}\min_{\forall\varphi,\eta,UL}: SC_{dy}^2 = {} & \frac{N_{dy}}{(1+r_i)^y}\sum_{t\in\mathcal{T}}\sum_{\phi\in\Phi_{dy}}\lambda_\phi\Big(w_l\sum_{l\in\mathcal{L}} r_l f_{l\phi t} \\ & + w_u\sum_{l\in\mathcal{L}}(up_{l\phi t}^{+}+up_{l\phi t}^{-}+uq_{l\phi t}^{+}+uq_{l\phi t}^{-})\Big)\end{aligned} \tag{19a}$$

$$\text{subject to: } (12),(15c),(15d), \tag{19b}$$
$$L(\Delta A_l^2) \ge a_k \Delta A_l + b_k, \forall k \in \{1,...,K_2\}, \forall l \tag{19c}$$
$$0 \le I_l^t \le (I_l^{max})^2 + 2I_l^{max}\Delta A_l + L(\Delta A_l^2), \forall l \tag{19d}$$
$$0 \le I_l^b \le (I_l^{max})^2 + 2I_l^{max}\Delta A_l + L(\Delta A_l^2), \forall l \tag{19e}$$
$$\begin{aligned}& R_{ldy}=R_l^* : \mu_{ldy}, C_{ldy}=C_l^* : \vartheta_{ldy}, \\ & \Delta A_{ldy}=\Delta A_l^* : \iota_{ldy}, \qquad \forall l, \forall d, \forall y\end{aligned} \tag{19f}$$

$$\Psi_{dy}^{(n)} = \big[SC_{dy}^{2*} - \sum_{l\in\mathcal{L}} (\mu_{ldy}(R_l - R_l^*) + \vartheta_{ldy}(C_l - C_l^*) + \iota_{ldy}(\Delta A_l - \Delta A_l^*))\big], \forall d, \forall y, \forall n \quad (20)$$

The ESS power ratings, the ESS energy reservoirs, and the change of ampacity are fixed to the optimal solution values of the master problem as shown in (19f). μ_{ldy}, ϑ_{ldy}, ι_{ldy} are the corresponding dual values, which are used to construct the Benders cut as shown in (20). The variables with subscript d, y, n are defined for $\forall d \in \mathcal{D}$, $\forall y \in \mathcal{Y}$, $\forall n \in \mathcal{N}_2$, respectively. The upper bound of the 2nd stage problem, or UB_2, is calculated summing the variable investment cost and the subproblem costs (i.e., $UB_2 = \sum_{l\in\mathcal{L}}(ic_E^e C_l^* + ic_E^p R_l^*) + \sum_{l\in\mathcal{L}} \rho_l(\delta_2(\Delta A_l^*)^2 + (2\delta_2 I_l^{max} + \delta_1)\Delta A_l^*) + \sum_{y\in\mathcal{Y}} \sum_{d\in\mathcal{D}} SC_{dy}^{2*}$).

V. Simulations

The performance of the proposed methods is assessed on an existing Swiss 21kV distribution network with 55 nodes characterized by a large renewable generation capacity (see Fig. 5(a)). 2.7MWp of PV generation and 805kVA of hydro power generation are installed. The detailed information of the network can be found in [33]. The planning horizon is set to 10 years and we assume that the load consumption grows annually by 7% over the planning horizon (*i.e.*, r_g=0.07). The considered ESS assets for the ADN are Li-ion batteries. The battery cost parameters and possible ranges of ESS energy reservoir and power rating are shown in Table I. The candidate nodes for ESS installation are set according to the indications of the operator of this grid. In Table II, the fixed costs associated to the line investment are given differently depending on the type of connection, considering that the estimated cost for constructing underground cables is roughly 4 times higher than overhead lines [34]. Fig. 3 shows the fittings of conductor cost and line parameters according to the line ampacity. As shown in Fig. 3(a), a quadratic function exhibits a better fit quality for the data of conductor cost versus the line ampacity than a linear function. Thus, the conductor cost is modeled as the quadratic function of line ampacity and the associated equation and coefficients (δ_2, δ_1, and δ_0) are indicated on the graph. In Fig. 3(b), the equation of hyperbolic curve best fits to the line resistance data and associated coefficients (α_2^r, α_1^r, and α_0^r) are shown. Likewise, the linear sensitivity coefficients (Δx and Δb) for the change in reactance and susceptance are indicated in Fig. 3(c) and (d), respectively. The penalty cost for the dispatch error is assumed to be \$897/MWh, which corresponds to the 99.9th percentile of the real imbalance price settled from 2018 to 2019 in the Swiss energy market [35]. The chosen price coefficient is notably higher than a typical price settled in the energy markets to secure a sufficient level of ADN dispatchability. The weight coefficients for grid losses and unserved energy are given as 6k/MWh and 100k/MWh, respectively. The seasonal variation of the prosumption over a year is modeled by 8 typical day-types. A prosumption forecast is assumed to be provided by a reliable forecasting methodology for each day-type. To model the prediction uncertainties for each day-type prosumption forecast, 1000 scenarios are generated with equal probabilities based on the assumption that the prosumption profile follows a normal distribution [6]. Then, by applying the K-medoids clustering technique [38], the scenarios are clustered into 10 scenarios[9]. We solve a planning problem using the determined operating scenario set to achieve the optimal level of dispatchability of ADNs by allocating ESS assets. Moreover, the line reinforcement is co-optimized along with the ESS allocation to consider the grid losses and the expected energy not served (EENS) while complying with the grid constraints such as nodal voltage limits and the line ampacity constraints. The optimization problems are solved using the solver MOSEK via the MATLAB interface YALMIP. The simulations are carried out on a desktop PC equipped with an Intel® Xeon® Gold CPU at 2.1GHz and with a physical system memory of 128 GB.

First, we show the performance of the planning tool considering both ESS assets and line reinforcement and analyze the trend of investment decisions with respect to varying PV penetration levels. Then, the performance of the solution approach based on the modified Benders approach is demonstrated by comparing it in terms of computation time and the planning result with the solution approach used in [39] and [13]. Moreover, the planning tool is tested on networks of different sizes ranging from 25 nodes to 123 nodes to show its scalable applicability.

TABLE I
ESS Parameter and Candidate Nodes for Simulation

Maximum power rating per site	4MVA	Maximum energy reservoir per site	7MWh
Installation cost for power rating	\$200/kVA	Installation cost for energy reservoir	\$300/kWh
Capital investment cost per site		\$0.1M	
ESS candidate nodes		4, 16, 27, 41, 45	

TABLE II
Parameters Related to Line Reinforcement

Fixed cost for overhead lines	\$0.12M/km [36]
Fixed cost for underground cables	\$0.48M/km [37]

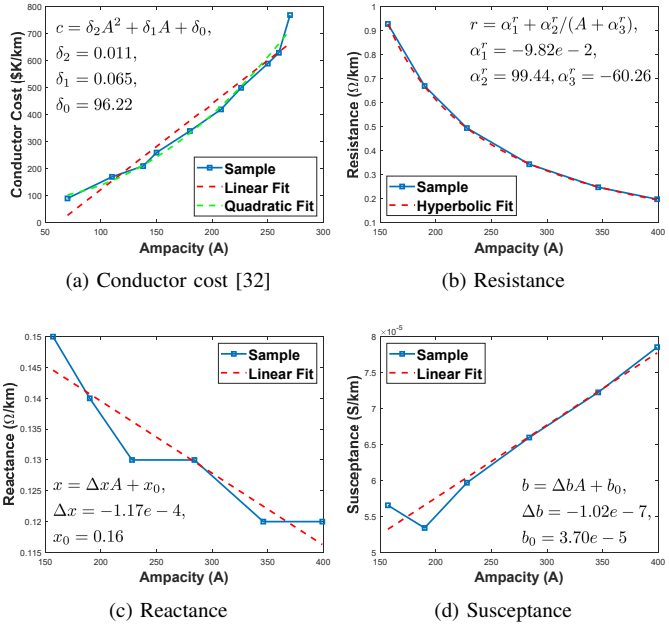

(a) Conductor cost [32] (b) Resistance

(c) Reactance (d) Susceptance

Fig. 3. Fitting of line parameters by the function of ampacity

[9]The number of reduced scenarios is set considering the similarity of the original scenarios and the reduced scenario sets based on the algorithm suggested in [13].

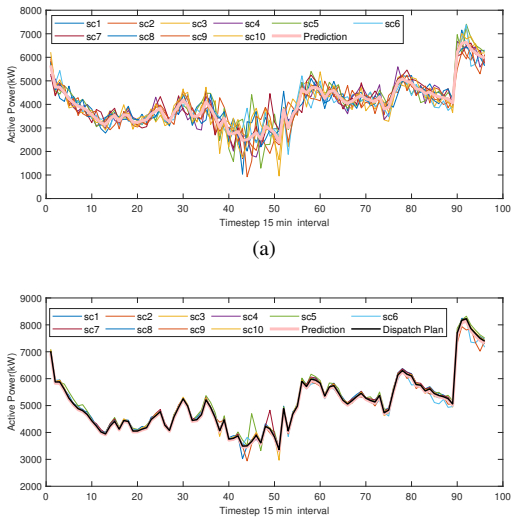

Fig. 4. Dispatch result of Day 1: (a) Aggregated prosumption scenarios and prosumption prediction, (b) Power flow through GCP of scenarios, prosumption prediction and dispatch plan (Imbalance price : $897/MWh).

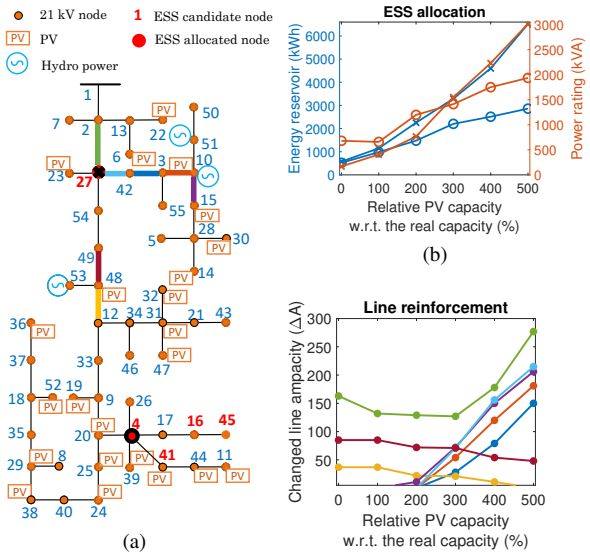

Fig. 5. (a) Topology with ESS allocation and line reinforcement, (b) ESS allocation (2nd block problem), (c) Line reinforcement (2nd block problem)

A. Planning results with different levels of PV capacities

We solve the planning problem considering various levels of PV capacities, while 100% of PV capacity corresponds to the existing PV capacity in the considered network. Fig. 4 shows the dispatch operation result of day-type 1 considering 100% of PV capacity. Fig. 4(a) demonstrates the aggregated prosumption scenarios along with the aggregated prosumption prediction, whereas Fig. 4(b) represents the dispatch result after investing both on ESS installation and line reinforcement. Thanks to the proposed planning strategy, the dispatch result shows that the power flow at the GCP of all scenarios follows the dispatch plan with the dispatch error determined by the optimal dispathability level of ADN. To address the impact of the PV generation uncertainty, different levels of PV capacity (*i.e.*, 0-500% of the existing PV capacity within the ADN) are given to the planning problem. The locations of ESSs and lines to be reinforced are determined as Fig. 5(a). As shown in Fig. 5(b), the ESSs allocated at Node 4 and Node 27 increase in their power ratings and energy reservoir with PV capacity. The capacity of ESS at Node 27 enlarges more with respect to the increasing PV levels than the ESS at Node 4, in order to compensate for the uncertainty of PV generation mostly attributed to Node 15, where the PV panels with the biggest capacity are located (1.6MWp at 100% of the existing PV capacity). In Fig. 5(c), the ampacity changes of the lines indicated with bold-colored lines in Fig. 5(a) are shown. A decrease in ampacity change is observed in the line between Node 48 and 12 (Line 48-12) and Line 49-48 as the PV penetration level increases. This is because the load consumption is mainly satisfied locally by the generation from nearby PV generation units, rather than by the power infeed from the main branch. On the other hand, four lines connecting the main branch (leading to GCP) and Node 15: Line 27-42, Line 42-3, Line 3-10, and Line 10-15, get updated starting from 300% and 200% of PV capacities, respectively, to support the increasing reverse power flow fed by the PV generation from Node 15. Lastly, the ampacity change of Line 2-27 decreases until the PV penetration level reaches 300% thanks to the local generation satisfying the load consumption. As the total PV generation level grows to more than 300%, the excessive PV generation as well as the increased dispatch of bigger ESS at Node 27 increase the power flow through the main branch, increasing the required ampacity change of Line 2-27. Finally, Fig. 6(a) and Fig. 6(b) show the comparison of the total cost related to the operation (imbalance, grid losses and unserved energy) and investment under different PV capacities. Fig. 6(a) demonstrates the cost of imbalance penalty and investment with and without ESS allocation (Noted as 'EX' and 'EO' which represent the planning case without ESS and with ESS, respectively) determined in the 1st block problem. The imbalance penalty cost without ESS installation increases drastically along with the level of PV capacity within the ADN. As a result of optimized ESS allocation, the imbalance cost is expected to be less than one-tenth of the default case in all PV capacities cases. Indeed, the investment cost associated with ESS allocation increases with larger PV capacity to achieve the optimal level of dispatchability. As shown in Fig. 6(b), the investment cost related to the ESS allocation and the line reinforcement increases with the increasing PV capacity. The cost related to EENS stays negligible until PV capacity of 300% but increases distinctively by curtailing excessive PV generation at the PV capacities of 400% and 500%.

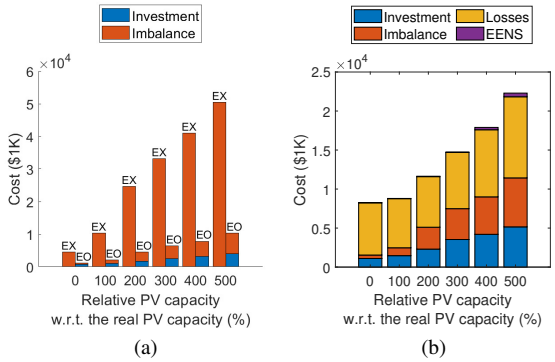

Fig. 6. Obtained optimal cost value of (a) First block problem, (b) Second block problem

B. Numerical assessment on the effect of separation of siting and sizing problems

In this section, we compare the planning result as well as the computational performance of the two solution approaches: Approach 1, where the siting and sizing decisions are made

TABLE III
THE PLANNING RESULTS COMPARISON (APPROACH 1 VS. APPROACH 2

	Approach 1			Approach 2		
ESS allocation (Node #)	4		27	4		27
Power rating (kVA)	700		341	673		387
Energy reservoir (kWh)	967		1202	1028		1151
Reinforced lines	48-12	2-27	48-49	48-12	2-27	48-49
Δampacity (ΔA)	36	133	85	37	133	85
Total cost ($M)	8.794			8.799		

together (*i.e.*, the Benders decomposition approach used in [39] and [13]), and Approach 2, where the siting and sizing decisions are made sequentially (*i.e.*, the proposed approach in this paper.) As shown in Fig. 7(a), by employing Approach 1, the evolution of the total cost over Benders iterations shows an unstable trajectory with the change of binary investment variables, which leads to slow convergence. On the other hand, in Approach 2, the Benders cut built in the 1st stage of 2nd block narrows down the binary solution space more effectively based on the evaluation of the best possible investment and operation decision with the given site decisions. Then, with the fixed sites, the 2nd stage problem converges faster to the best size solution. In this way, the zigzagging behavior in the evolution of the total planning cost is notably reduced as shown in Fig. 7(b) and Fig. 7(c). The texts on the graphs show the comparison of the computation time between Approach 1 and Approach 2. The average computation times for solving a subproblem of Approach 1 are similar to those of the 1st and 2nd stages in Approach 2. On the other hand, the average computation time of master problems for Approach 1 is significantly bigger than those for Approach 2 due to the sets of benders cuts accumulatively added with the large number of benders iterations for Approach 1. The sum of the Benders iteration number of the 1st and 2nd stage of Approach 2 is smaller than the iteration number of Approach 1, verifying the superior performance of Approach 2 in the convergence speed of the algorithm. Indeed, as shown in Table III, the planning results obtained from both approaches show a negligible difference in terms of the ESS allocation, line reinforcement results, and objective costs. Based on the result, it can be concluded that the Approach 2 is computationally more efficient than Approach 1 when numerous binary investment decisions have to be tackled.

C. Scalability analysis regarding the network size

The proposed method has been applied to distribution networks of various sizes to analyze its scalability. The number of dispatch intervals was 24, and 4 day-types were considered. Other parameter settings for the analysis are the same as the ones adopted in Sec. V. All the network data can be found in [33] and [40]. Fig. 8 reports the average computation time per Benders iteration (denoted by 'BI' in the figure) and the number of Benders iterations (including both 1st and 2nd stage of the 2nd block problem) to solve the planning problems for available IEEE benchmark feeders with the number of nodes ranging from 25 to 123. Fig. 8.(a) and Fig. 8.(b) show respectively the trend of the average computation time per Benders iteration and total computation time concerning the system sizes. The results verify the tractability of the planning model for distribution network feeders of a realistic size.

In each Benders iteration, solving the subproblem (i.e., operation problem) takes the most computation time due to numerous operational variables and constraints determined by

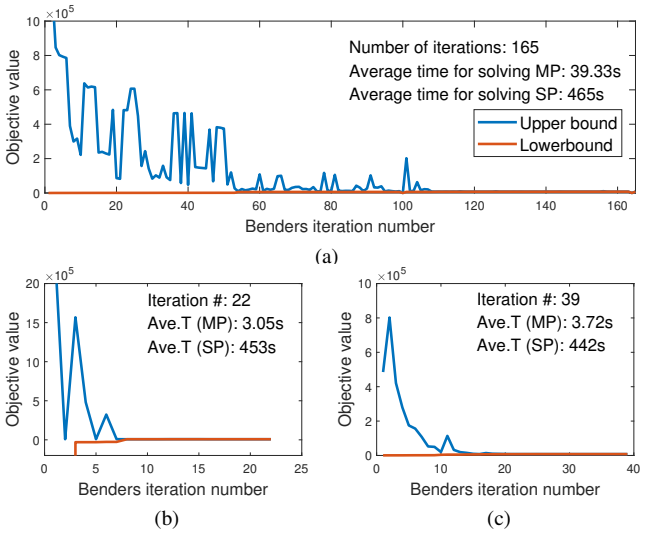

Fig. 7. Convergence of Benders decompostion: (a) Approach 1, (b) 1st stage (Approach 2), (c) 2nd stage (Approach 2)

the system size. However, as shown in Fig. 8.(a), the average computation time per Benders iteration does not increase linearly with the system size. It implies that the computation time depends not only on the system (i.e., problem) size but also on the solution space, which is largely affected by the network's operating condition. Furthermore, Fig. 8.(b) shows that the total computation time depends on the number of Benders iterations. For example, the difference in total computation time of 25-node system versus 55-node system is very small (i.e., around 5% of the total computation time for 25-node system) compared to that in average computation time per Benders iteration (i.e., around 115% of the average computation time per Benders iteration for 25-node system). It is attributed to the smaller number of total Benders iterations for the 55-node system in comparison to the 25-node system. Meanwhile, the total computation time for the 69-node system increased to more than 4 times compared to the 55-node system. In contrast, the total computation time for the 123-node system was 2.22 hours shorter than that with 69 nodes. The results indicate that the convergence speed of the proposed method is influenced by how the set of Benders cuts narrow down the solution space to identify the optimal solution. Given that the Benders cut is determined by the dual values obtained from solving the subproblems, the system operating condition significantly influences the optimal investment solution and the convergence speed.

Nodes #	Time/BI (h)	1st+2nd BI #	Total time (h)
25	0.29	43+22	18.61
55	0.61	12+20	19.67
69	1.14	59+16	85.28
123	1.22	28+40	83.06

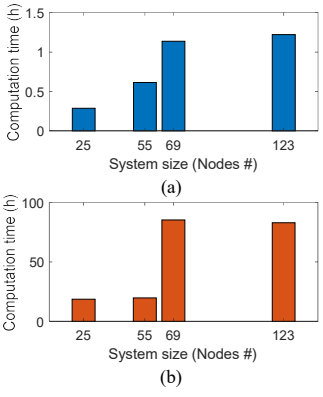

Fig. 8. (a) Average computation time per Benders iteration (BI) for distribution networks with different sizes, (b) Total computation time for distribution networks with different sizes

VI. Discussion on the limitation of the proposed method

The investment decisions are influenced by how accurately the scenarios model the stochasticity of the prosumption uncertainty and the seasonal variability. However, it is worth noting that the modeling of uncertainty is beyond the scope of this paper. In practice, the modeler should have a reliable forecasting and scenario generation tool.

Another limitation of the work is that the proposed method is specifically designed for radial networks. It is already proven that, for radial networks, if an optimal solution is obtained from the SOCP-relaxed OPF while the equality holds for (10e) (i.e., the inequality constraint associated with the line current), then it is equivalent to the optimal solution of the Branch flow model. Note that the phase angles of nodal voltages are relaxed in the Branch flow model. The phase angles can be recovered through the known angle recovery algorithm [25].

For meshed networks, the so-called cyclic condition, stating that the sum of the voltage angle differences for adjacent nodes should be zero (mod 2π) for any loop in the meshed network, must hold to recover an optimal solution of the original OPF from the optimal solution of its SOCP-relaxed model [25]. Hence, the application to meshed networks requires appropriate changes in the OPF formulation. This specific aspect constitutes our future work.

VII. Conclusion

This study presents a tool for the co-optimized planning of ESSs and lines reinforcement for ADNs to achieve their dispatchability. ESSs are employed to compensate for the uncertainty of the prosumption such that the realized power flow at the GCP can track a day-ahead computed dispatch plan. The line reinforcement is considered for investment to help satisfying the grid operational constraints. The line characteristics and the grid constraints associated with the line ampacity in the MAR-OPF model are adjusted with the change of line ampacity to reflect the impact of line reinforcement on the grid operation. The planning problem is reformulated such that the siting and sizing problems of ESSs and lines reinforcement are tackled sequentially by Benders decomposition. We assessed the performance of the proposed method on a real Swiss ADN with substantial levels of installed PV capacity. The results demonstrate that the proposed co-optimization framework can successfully guarantee the optimal level of dispatchability while securing the proper hosting capacity of the ADN under increasing load consumption and a large amount of distributed stochastic renewable generation. Moreover, the benefits associated to the separation of the siting and sizing in the planning problem of ESSs and lines reinforcement are numerically assessed by comparing the computation time and investment solution to the original planning problem. The computation time for solving the reformulated problem was one-third of that for the original problem while the difference between the investment solution and the total planning and expected operating costs of the two problems were negligible. Moreover, the simulations conducted on IEEE test networks and the real network of various sizes demonstrate that the proposed planning method is sufficiently scalable to be applied to networks of generic sizes.

VIII. Acknowledgement

This project is carried out within the frame of the Swiss Centre for Competence in Energy Research on the Future Swiss Electrical Infrastructure (SCCER-FURIES) with the financial support of the Swiss Innovation Agency (Innosuisse - SCCER program), Hitachi Energy, Switzerland, and ABB, Switzerland.

References

[1] B. Murugananthan, R. Gnanadass, and N. Padhy, "Challenges with renewable energy sources and storage in practical distribution systems," *Renew. Sust. Energ. Rev.*, vol. 73, pp. 125–134, 2017.

[2] S. Lavrijssen, A.-A. Marhold, and A. Trias, "The changing world of the dso in a smart energy system environment: Key issues and policy recommendations," *TILEC Discussion Paper*, no. 2018-015, pp. 1–98, 2016.

[3] S. Kim, M. Pollitt, Y. Jin, J. Kim, and Y. Yoon, "Contractual framework for the devolution of system balancing responsibility from the transmission system operator to distribution system operators," *EPRG Working Paper*, no. 1715, 2017.

[4] H. Gerard, E. I. R. Puente, and D. Six, "Coordination between transmission and distribution system operators in the electricity sector: A conceptual framework," *Utilities Policy*, vol. 50, pp. 40–48, 2018.

[5] G. Koeppel and M. Korpås, "Improving the network infeed accuracy of non-dispatchable generators with energy storage devices," *Electr. Pow. Syst. Res.*, vol. 78, no. 12, pp. 2024–2036, 2008.

[6] F. Sossan, E. Namor, R. Cherkaoui, and M. Paolone, "Achieving the dispatchability of distribution feeders through prosumers data driven forecasting and model predictive control of electrochemical storage," *IEEE Trans. Sustain. Energy*, vol. 7, no. 4, pp. 1762–1777, Oct 2016.

[7] M. Bozorg, F. Sossan, J.-Y. Le Boudec, and M. Paolone, "Influencing the bulk power system reserve by dispatching power distribution networks using local energy storage," *Electr. Power Syst. Res.*, vol. 163, pp. 270–279, 2018.

[8] M. Kalantar-Neyestanaki and R. Cherkaoui, "Coordinating distributed energy resources and utility-scale battery energy storage system for power flexibility provision under uncertainty," *IEEE Trans. Sustain. Energy*, 2021.

[9] "Directive (eu) 2019/944 of the european parliament and of the council of 5 june 2019 on common rules for the internal market for electricity and amending directive 2012/27/eu," *Official Journal of the European Union L 158*, vol. 62, pp. 125–199, 2019.

[10] O. H. Anuta, P. Taylor, D. Jones, T. McEntee, and N. Wade, "An international review of the implications of regulatory and electricity market structures on the emergence of grid scale electricity storage," *Renew. Sust. Energ. Rev.*, vol. 38, pp. 489–508, 2014.

[11] S. Ugarte, J. Larkin, B. Van der Ree, V. Swinkels, M. Voog, N. Friedichsen, J. Michaels, A. Thielmann, M. Wietschel, and R. Villafafila, "Energy storage: Which market designs and regulatory incentives are needed?" *Eur. Parliament Committee Ind., Res. Energy, Brussels, Belgium*, pp. 1–5, 2015.

[12] G. C. Gissey, P. E. Dodds, and J. Radcliffe, "Market and regulatory barriers to electrical energy storage innovation," *Renewable and Sustainable Energy Reviews*, vol. 82, pp. 781–790, 2018.

[13] J. H. Yi, R. Cherkaoui, and M. Paolone, "Optimal allocation of esss in active distribution networks to achieve their dispatchability," *IEEE Trans. Power Syst.*, 2020.

[14] R. C. Lotero and J. Contreras, "Distribution system planning with reliability," *IEEE Trans. Power Del.*, vol. 26, no. 4, pp. 2552–2562, 2011.

[15] J. F. Franco, M. J. Rider, M. Lavorato, and R. Romero, "Optimal conductor size selection and reconductoring in radial distribution systems using a mixed-integer lp approach," *IEEE Trans. Power Syst.*, vol. 28, no. 1, pp. 10–20, 2012.

[16] G. Munoz-Delgado, J. Contreras, and J. M. Arroyo, "Distribution network expansion planning with an explicit formulation for reliability assessment," *IEEE Trans. Power Syst.*, vol. 33, no. 3, pp. 2583–2596, 2017.

[17] B. Canizes, J. Soares, F. Lezama, C. Silva, Z. Vale, and J. M. Corchado, "Optimal expansion planning considering storage investment and seasonal effect of demand and renewable generation," *Renew. Energy*, vol. 138, pp. 937–954, 2019.

[18] X. Shen, M. Shahidehpour, Y. Han, S. Zhu, and J. Zheng, "Expansion planning of active distribution networks with centralized and distributed energy storage systems," *IEEE Trans. Sustain. Energy*, vol. 8, no. 1, pp. 126–134, 2016.

[19] M. Asensio, P. M. de Quevedo, G. Muñoz-Delgado, and J. Contreras, "Joint distribution network and renewable energy expansion planning considering demand response and energy storage—part i: Stochastic programming model," *IEEE Trans. on Smart Grid*, vol. 9, no. 2, pp. 655–666, 2016.

[20] P. M. de Quevedo, G. Munoz-Delgado, and J. Contreras, "Impact of electric vehicles on the expansion planning of distribution systems considering renewable energy, storage, and charging stations," *IEEE Trans. on Smart Grid*, vol. 10, no. 1, pp. 794–804, 2017.

[21] H. Saboori *et al.*, "Multistage distribution network expansion planning considering the emerging energy storage systems," *Energy Convers. Manag.*, vol. 105, pp. 938–945, 2015.

[22] R. Hemmati, H. Saboori, and M. Jirdehi, "Multistage generation expansion planning incorporating large scale energy storage systems and environmental pollution," *Renew. Energy*, vol. 97, pp. 636–645, 2016.

[23] D. M. Greenwood, N. S. Wade, P. C. Taylor, P. Papadopoulos, and N. Heyward, "A probabilistic method combining electrical energy storage and real-time thermal ratings to defer network reinforcement," *IEEE Trans. Sustain. Energy*, vol. 8, no. 1, pp. 374–384, 2016.

[24] C. Abbey, A. Baitch, B. Bak-Jensen, C. Carter, G. Celli, K. El Bakari, M. Fan, P. Georgilakis, T. Hearne, L. N. Ochoa *et al.*, *Planning and optimization methods for active distribution systems*. CIGRE (International Council on Large Electric Systems), 2014.

[25] S. H. Low, "Convex relaxation of optimal power flow—part i: Formulations and equivalence," *IEEE Trans. Control Netw. Syst.*, vol. 1, no. 1, pp. 15–27, 2014.

[26] J. M. Home-Ortiz, O. D. Melgar-Dominguez, M. Pourakbari-Kasmaei, and J. R. S. Mantovani, "A stochastic mixed-integer convex programming model for long-term distribution system expansion planning considering greenhouse gas emission mitigation," *International Journal of Electrical Power & Energy Systems*, vol. 108, pp. 86–95, 2019.

[27] H. Haghighat and B. Zeng, "Stochastic and chance-constrained conic distribution system expansion planning using bilinear benders decomposition," *IEEE Trans. Power Syst.*, vol. 33, no. 3, pp. 2696–2705, 2017.

[28] M. Nick, R. Cherkaoui, J. L. Boudec, and M. Paolone, "An exact convex formulation of the optimal power flow in radial distribution networks including transverse components," *IEEE Trans. Autom. Control*, vol. 63, no. 3, pp. 682–697, March 2018.

[29] M. Nick, R. Cherkaoui, and M. Paolone, "Optimal allocation of dispersed energy storage systems in active distribution networks for energy balance and grid support," *IEEE Trans. Power Syst.*, vol. 29, no. 5, pp. 2300–2310, 2014.

[30] E. Namor, D. Torregrossa, F. Sossan, R. Cherkaoui, and M. Paolone, "Assessment of battery ageing and implementation of an ageing aware control strategy for a load leveling application of a lithium titanate battery energy storage system," in *2016 IEEE 17th Workshop on COMPEL*. Ieee, 2016, pp. 1–6.

[31] E. Stai, L. Reyes-Chamorro, F. Sossan, J.-Y. Le Boudec, and M. Paolone, "Dispatching stochastic heterogeneous resources accounting for grid and battery losses," *IEEE Trans. on Smart Grid*, vol. 9, no. 6, pp. 6522–6539, 2017.

[32] Z. Zhao and J. Mutale, "Optimal conductor size selection in distribution networks with high penetration of distributed generation using adaptive genetic algorithm," *Energies*, vol. 12, no. 11, p. 2065, 2019.

[33] J. H. Yi. (2022) 55nodes-swiss-distribution-grid. [Online]. Available: https://github.com/DESL-EPFL/55nodes-Swiss-distribution-grid

[34] S. A. Fenrick and L. Getachew, "Cost and reliability comparisons of underground and overhead power lines," *Utilities Policy*, vol. 20, no. 1, pp. 31–37, 2012.

[35] Swissgrid. (2020) The prices for balance energy. [Online]. Available: https://www.swissgrid.ch/en/home/customers/topics/bgm/balance-energy.html

[36] I. Ziari, G. Ledwich, A. Ghosh, and G. Platt, "Optimal distribution network reinforcement considering load growth, line loss, and reliability," *IEEE Trans. Power Syst.*, vol. 28, no. 2, pp. 587–597, 2012.

[37] Z. Zhu, S. Lu, B. Gao, T. Yi, and B. Chen, "Life cycle cost analysis of three types of power lines in 10 kv distribution network," *Inventions*, vol. 1, no. 4, p. 20, 2016.

[38] A. K. Jain, R. C. Dubes *et al.*, *Algorithms for clustering data*. Prentice hall Englewood Cliffs, NJ, 1988, vol. 6.

[39] M. Nick, R. Cherkaoui, and M. Paolone, "Optimal planning of distributed energy storage systems in active distribution networks embedding grid reconfiguration," *IEEE Trans. Power Syst.*, vol. 33, no. 2, pp. 1577–1590, March 2018.

[40] J. H. Yi. (2022) Ieee-benchmark-distribution-grids. [Online]. Available: https://github.com/DESL-EPFL/IEEE_benchmark_distribution_grids

Ji Hyun Yi received the B.Sc. degree in electrical and electronic engineering from Yonsei University, South Korea, in 2015. Then, she received the M. Sc. Degree in electrical engineering from the National University of Seoul in 2018. She is currently a PhD student at the Distributed Electrical Systems Laboratory of the Swiss Federal Institute of Technology Lausanne (EPFL). Her research interests include distribution system planning for procurement of local system flexibility.

Rachid Cherkaoui (Senior Member, IEEE) received the M.Sc. and Ph.D. degrees in electrical engineering from the Swiss Federal Institute of Technology in Lausanne (EPFL), Lausanne, Switzerland, in 1983 and 1992, respectively. He is currently a Senior Scientist with EPFL, leading the Power Systems Group. He has authored and coauthored more than 150 scientific publications. His research interests include electricity market deregulation, distributed generation and storage, and power system vulnerability mitigation. Dr. Cherkaoui is a member of technical program committees of various conferences and was a member of CIGRE TF's and WG's. He was the IEEE Swiss Chapter Officer from 2005 to 2011.

Mario Paolone (M'07, SM'10, F'22) received the M.Sc. (Hons.) and Ph.D. degrees in electrical engineering from the University of Bologna, Italy, in 1998 and 2002. In 2005, he was an Assistant Professor in power systems with the University of Bologna, where he was with the Power Systems Laboratory until 2011. Since 2011, he has been with the Swiss Federal Institute of Technology, Lausanne, Switzerland, where he is Full Professor and the Chair of the Distributed Electrical Systems Laboratory. His research interests focus on power systems with particular reference to real-time monitoring and operational aspects, power system protections, dynamics and transients. Dr. Paolone's most significant contributions are in the field of PMU-based situational awareness of Active Distribution Networks (ADNs) and in the field of exact, convex and computationally-efficient methods for the optimal planning and operation of ADNs. Dr. Paolone was the founder Editor-in-Chief of the Elsevier journal Sustainable Energy, Grids and Networks.

Dmitry Shchetinin (Member, IEEE) received the B.Eng. degree in 2010 and the M.Eng. degree from Moscow Power Engineering Institute, Moscow, Russia, the M.Sc. degree from Carnegie Mellon University, Pittsburgh, PA, USA, in 2015, and the Ph.D. degree from the Swiss Federal Institute of Technology, Zurich, Switzerland, in 2018. He is currently a Scientist with Hitachi Energy Research Center, Zurich, Switzerland, where he works on computational methods for power system control and optimization.

Katarina Knezovic (Member, IEEE) received the B.Sc. and M. Sc. degree in electrical engineering from University of Zagreb, Croatia, in 2011 and 2013 respectively, and the PhD in electrical engineering from the Technical University of Denmark in 2017. She is currently working as a Senior Scientist at Hitachi Energy Research in Switzerland. Her research interests include power system control and optimization, integration of renewable energy and e-mobility, and data-driven methods for power systems.